X-ray source trajectories and their R-line coverage for long-object CB imaging with a C-arm system

Zhicong Yu, Frédéric Noo, Frank Dennerlein, Günter Lauritsch, Joachim Hornegger

***Abstract*—The geometry of the helix has been successfully applied in diagnostic CT for extended volume imaging without cone-beam artifacts. However, it cannot be used for C-arm systems due to the absence of slip-ring technology. For this reason, the reverse helix was proposed recently for C-arm systems, but efficient reconstruction from axially-truncated data collected on such a helix appears to be challenging. The main difficulty comes from the the missing R-line coverage in the central region of the scanned object. More specifically, the reverse helix is such that the theories that have been found for efficient handling of axial truncation cannot be applied, because large portions of the object are not intersected by R-lines**

In this work, we revisit the option of performing extended field-of-view imaging using a sequence of circular short-scans connected by line segments. We find that the R-line coverage is insufficient for a central region of interest when a line-segment is tightly fit between parallel circular arcs. On the other hand, extension of the line beyond the circular arc helps to increase R-line coverage in the central region of interest. Therefore, we propose a trajectory composed of two parallel circular arcs connected by an extended line. This trajectory does have a nice R-line coverage inside the ROI, but it has a discontinuity at the endpoints of the line. To overcome this problem, we suggest replacing the two parallel circular arcs by two helices, which can be duplicated along the axial axis conveniently and which, moreover, keeps the trajectory continuous and thus is more practical.

I. Introduction

Over the decade, cone-beam (CB) computed tomography has become a valuable tool in interventional radiology. Its success stems from its ability to provide the medical doctor with immediate feedback during a clinical procedure, thereby allowing on-the-fly adjustments. So far, circular data acquisition has been used, but more sophisticated geometries are being considered due to the problem of cone-beam artifacts and also due to limited volume coverage.

An attractive geometry for extended volume imaging with no cone-beam artifacts is the helix. This geometry has been very successful in diagnostic CT, but is unfortunately not practical for interventional radiology. The problem is the need for slip-ring technology, which is difficult to use (if possible at reasonable cost) with C-arm systems. To perform extended volume imaging with a C-arm system, another geometry must be found. Many options are possible, from using a combination of circles and lines, to using a reverse helix, as suggested by the group of X. Pan at the University of Chicago [1]. The reverse helix has many merits, but efficient reconstruction from axially-truncated data collected on such a helix appears to be challenging [1], [2]. The main difficult comes from the R-lines not covering the whole scanned object (an R-line is any line segment that connects two source positions together). More specifically, the reverse helix is such that the theories that have been found for efficient handling of axial truncation [3]–[6] cannot be applied, because large portions of the object are not intersected by R-lines.

In this work, we revisit the option of performing extended field-of-view imaging using a sequence of circular short-scans connected by line segments. In particular, we investigate R-line coverage with the goal of finding source-trajectory parameters such that a central region-of-interest within the object is fully covered by R-lines.

The paper is organized as follows. First, we describe the data acquisition geometry of interest. Next, we discuss R-line coverage resulting from two parallel circular arcs, and also R-line coverage resulting from connecting a line orthogonally to the endpoint of a circular arc. From there, we are then able to present the R-line coverage for the whole data acquisition geometry. Our results show that some parameters allow full coverage of a region-of-interest, but these parameters unfortunately come with practical implementation concerns. We discuss these concerns and potential remedies in the last section.

II. Data acquisition geometry

We consider extended volume imaging using periodic duplicates of a source trajectory consisting of two circular arcs connected by a segment of line. The patient is assumed to lie along the z-axis, the arcs are in parallel planes that are orthogonal to this axis, and the line is orthogonal to each arc through one of its endpoints. Figure 1 depicts this trajectory. Two options are considered: (a) the line is spatially limited by the arcs, (b) the line extends beyond the arcs. Figure 1 also shows how each circular arc is oriented relative to x and y-axes that form together with the z-axis a Cartesian system of coordinates. The distance in z between the arcs is $2\,H$, the radius of the arcs is R, and the line extension in the second path option is Δh on each side. Also, the plane $z = 0$ is chosen

Z. Yu and F. Noo are with the Department of Radiology, University of Utah, 729 Arapeen Drive, Salt Lake City, UT 84102 USA (e-mail: zyu@ucair.med.utah.edu, noo@ucair.med.utah.edu).

F. Dennerlein and G. Lauritsch are with Siemens AG, Healthcare Sector, 91301 Forchheim, Germany.

J. Hornegger is with the Chair of Computer Science 5 (Pattern Recognition), University of Erlangen-Nuremberg, 91058 Erlangen, Germany.

This work was partially supported by a grant of Siemens AG, Healthcare Sector and by the U.S. National Institutes of Health (NIH) under grant R21 EB009168. The concepts presented in this paper are based on research and are not commercially available. Its contents are solely the responsibility of the authors and do not necessarily represent the official views of the NIH.

to be at mid-distance between the two arcs. To avoid confusion with other arcs that will appear later in the discussion, from now on we will use the term S-arcs to refer to the arcs forming the source trajectories.

III. Elemental R-line Coverage

In this section, we first discuss the R-line coverage resulting from connecting points from one arc to the other arc. Next, we discuss the additional coverage resulting from connecting points on the line to points on the arcs. Note that our data acquisition is symmetric relative to the $z = 0$ plane. Therefore, the R-line coverage at position $z = z_0$ is the same as the coverage at $z = -z_0$ for any $0 \leq z_0 \leq H$. Hence, we only discuss R-line coverage at positions $z \geq 0$.

A. Arc-to-arc coverage

To understand the R-line coverage in this case, we start by considering the simpler case where each S-arc has a length of 360 degrees. Figure 2 shows how the R-line coverage can be found in this case. Location $z = 0.2\,H$ is used for the illustration but a similar result would be obtained at any other z-location. Basically, we take a point on the upper S-arc, called A^i_+, and connect it to all points on the lower S-arc. Doing so, we create the surface of a cone that intersects the plane $z = 0.2\,H$ along a circle. This circle defines the R-line coverage coming from A^i_+ in the plane $z = 0.2\,H$. By moving A^i_+ along the upper S-arc, we obtain additional circles, as shown on the right side of Figure 2. The union of these circles is the full R-line coverage in the plane $z = 0.2\,H$; this union is an annular region with external boundary, $\mathcal{C}$, corresponding to the intersection between plane $z = 0.2\,H$ and the cylinder on which the source trajectory is drawn.Now, we consider the case where the S-arcs are shorter. A length of 230 degrees is used for the illustrations; similar results would be observed with other short-scan lengths. Figure 3 shows the coverage in plane $z = 0.2\,H$, whereas figure 4 illustrates the coverage at $z = 0$.

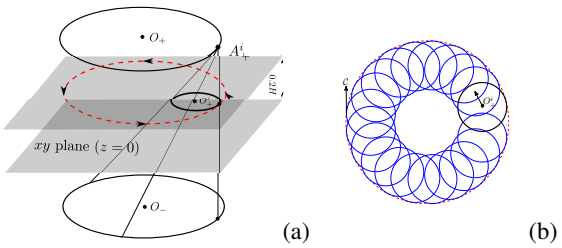

Fig. 2. Arc-to-arc R-line coverage when the length of the arcs is 360 degrees. (a) Coverage in plane $z = 0.2\,H$ due to one point from the upper S-arc; this coverage is a circle centered on a point denoted as O^i_+ in the figure. (b) Coverage in the same plane as on the left, but due to several points on the upper S-arc.

First, comparing figure 2a with figure 3a, we see that the coverage from A^i_+ is not a full circle anymore, it is a circular arc, which we refer to as an R-arc to avoid ambiguity between such an arc and the S-arcs that form the source trajectory. By moving A^i_+ along the upper S-arc, we obtain a union of R-arcs that defines the R-line coverage at $z = 0.2H$. Identifying the region covered by this union is not too complex. First, we observe that the endpoints of the R-arc, A_h and B_h, move along two arcs. The arc along which A_h moves is shown in figure 3c; it is the intersection between the plane $z = 0.2\,H$ and the (open) cone surface that results from connecting A^i_- to the upper S-arc, where A^i_- is the point on the lower arc that is at the same (x, y) location as A^i_+. The arc along which B_h moves is shown in figure 3d; this arc is created from the cone based on the upper S-arc and the endpoint A^e_- on the lower S-arc. Secondly, compared to figure 3, we illustrate the variation of the R-line coverage along the z-axis by looking at the plane $z = 0$, as shown in figure 4. Using the same process as in figure 3, we take a point A^i_+ on the upper S-arc and connect it to the lower S-arc; with this procedure, we get a surface consisting of a partial cone, which intersects with the plane $z = 0$ along a partial circular arc whose two endpoints are denoted as A_h and B_h. By moving A^i_+ along the upper S-arc, we acquire the combination of R-arcs that forms the R-line coverage in the plane $z = 0$, as illustrated in figure 4b. The identification of the R-line coverage in the plane $z = 0$ could be performed similarly to the case depicted in figure 3. The difference is that the orbit of the endpoint A_h is the R-arc itself corresponding to the point A^i_+ on the upper S-arc, as shown in figure 4a; while the point B_h follows the dashed partial circular arc as illustrated in figure 4c. Both tracks of points A_h and B_h go through the center of the cylinder, on whose surface the two S-arcs are located. Figure 4 also contains the results of a numerical simulation. Combining the information in figure 3, we observe that in planes orthogonal to the z-axis, as $|z|$ increases, the R-line coverage corresponding to one point on the upper S-arc becomes smaller and the orbits of the endpoints of the R-arc become larger, and thus the R-line coverage around z axis becomes worse.

B. Arc-to-line coverage

In this subsection, we investigate another elemental data acquisition geometry: a line orthogonally attached to a partial circular arc at one of its endpoints. Recall from figures 1a and 1b that two S-arcs are symmetric relative to the plane $z = 0$. In this case, the R-line coverage resulting from connecting the points on the line to points on the upper S-arc is symmetric to that obtained from connecting the points on the line to the points on the lower S-arc. Therefore, we consider here only the R-line coverage that results from the line located above the S-arc. Figure 5 depicts this R-line coverage. Here, we used location $z = 0$ and angular coverage 230° as an example, but a similar result could be obtain at any location $-H \leq z \leq H$. Figure 5b shows the R-line coverage resulting from the numerical simulation.

As observed, the R-line coverage of the arc-to-line in the plane $z = 0$ is a partial disk. Compared to Figure 4, we can see the outline of the partial disk is actually the union of the R-lines connecting the point A^i_+ to the lower S-arc in Figure 4. The union of all the disks along the line is a cone whose base is bounded by the lower S-arc and with peak at the

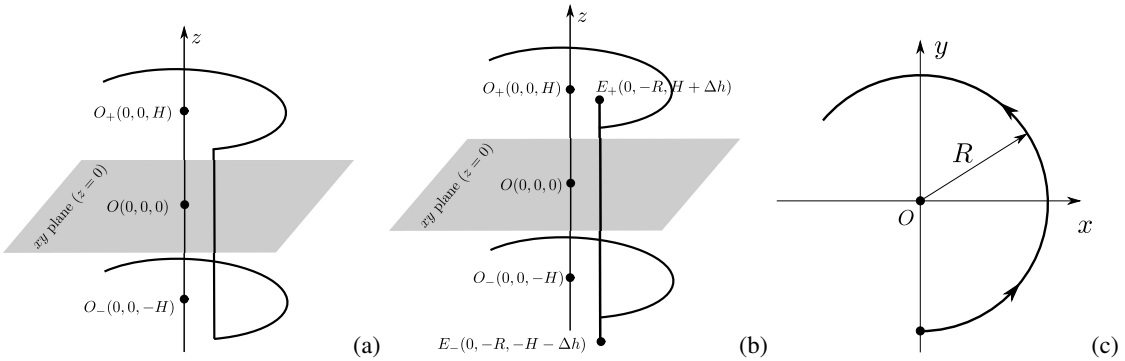

Fig. 1. Data acquisition geometry. Extended volume imaging is performed using duplicates of a path consisting of two arcs plus a line. Two options are considered for this path: (a) the line is tightly fit between the arcs, so that each endpoint of the line corresponds to one endpoint of an arc; (b) the line extends beyond the arcs by a distance Δh on each side. (c) Orthogonal projection of the source trajectory onto the $x-y$ plane.

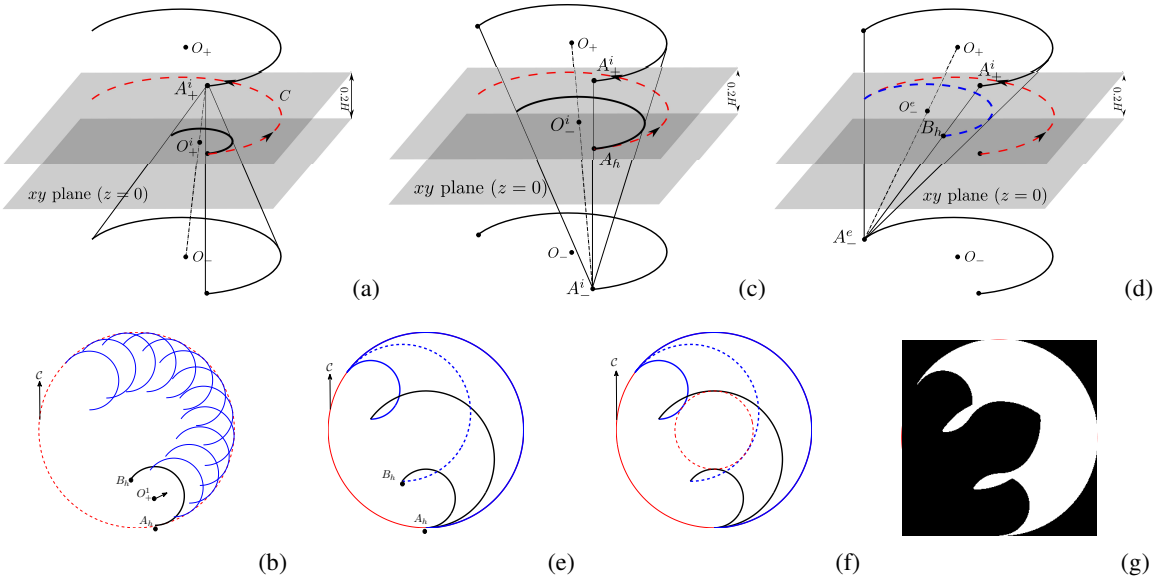

Fig. 3. Arc-to-arc R-line coverage when the length of the arcs is 230 degrees. (a) Coverage in plane $z=0.2H$ due to one point from the upper S-arc; this coverage is a partial circular arc centered on a point denoted as O^i_+ in the figure. (b) Coverage in the same plane as in (a), but due to several points on the upper S-arc. (c) The track (the solid arc centered on the point O^i_-) which A_h follows when moving point A^i_+ along the upper S-arc. It is the intersection between the cone surface due to A^i_- and the plane $z=0.2H$. (c) The track (the dashed arc centered on the point O^e_-) of B_h when moving the point A^i_+ along the upper S-arc. (e) Combination of arcs from (b), (c) and (d). (f) Additional outlines are needed for R-line coverage of the two S-arcs. The reason is that when the R-arc moves along the C, due to the large angular coverage of the S-arcs, A_h and B_h are not always the furthest point to the z axis. (g) the numerical simulation result.

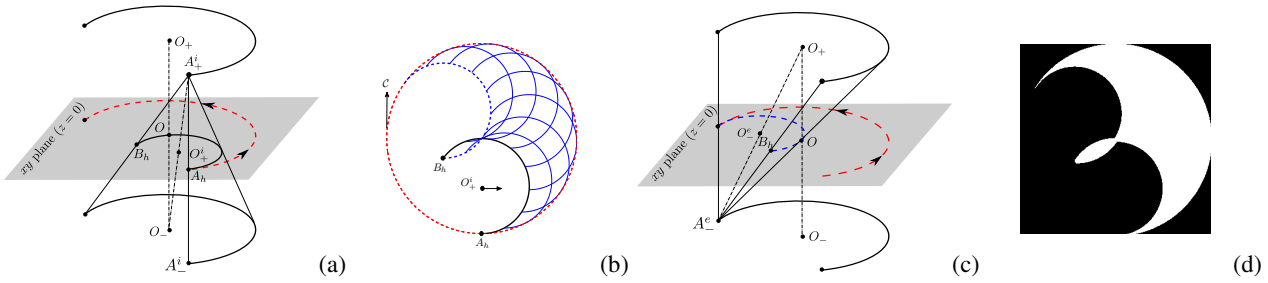

Fig. 4. Arc-to-arc R-line coverage when the length of the arcs is 230 degrees. (a) Coverage in plane $z=0$ due to one point from the upper S-arc; this coverage is a partial circular arc centered on a point O^i_+. (b) Coverage in the same plane as in (a), but due to several points on the upper S-arc. (c) The track (the dashed partial circular arc) of B_h when A^i_+ moves along the upper S-arc. (d) the numerical simulation result.

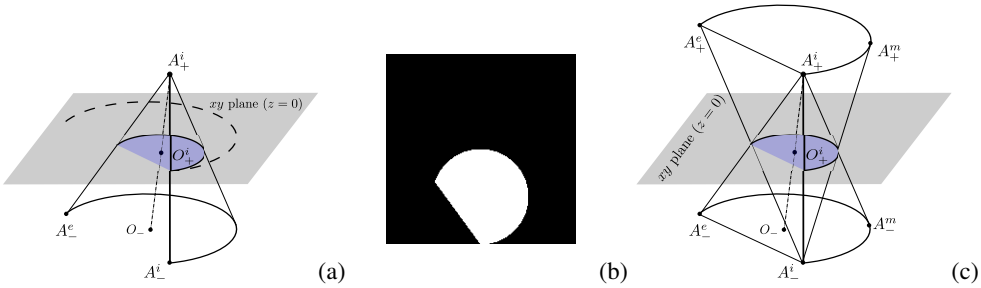

Fig. 5. Arc-to-line R-line coverage when the length of the arcs is 230 degrees. The line is attached to one of the endpoints of the S-arc. (a) Coverage in plane $z = 0$ due to one point A^i_+. This coverage is a partial disk centered on a point denoted as O^i_+. (b) the numerical simulation result. (c) the union of two symmetric cones of R-line coverage, which is resulting from connecting points on the line to the points on the two S-arcs.

point A^i_+. Due to the symmetry of the trajectory as illustrated in Figure 1b, the R-line coverage between the line and the upper S-arc would be an upside-down cone, congruent to that between the line and the lower S-arc. The union of these two cones intersected with the $z = 0$ plane is shown in Figure 5c. As we can see, the R-line coverage resulting from connecting points on the line to the two R-arcs has its minimum in the plane $z = 0$ and increases when $|z|$ becomes larger.

To give a better understanding of the relation between the R-line coverage of the two R-arcs and that of a line and an S-arc, we offer an illustration in Figure 6. Here we choose the plane at height $z = 0.2H$ as an example, but a similar result could be obtained for any other locations with $-H \leq z \leq H$. Figure 6 depicts the combination of R-lines from the elemental trajectories: arc-to-arc and arcs-to-line . We observe that the R-line coverage from the line and the S-arc and the R-line coverage from the two S-arcs compensate each other quite well.

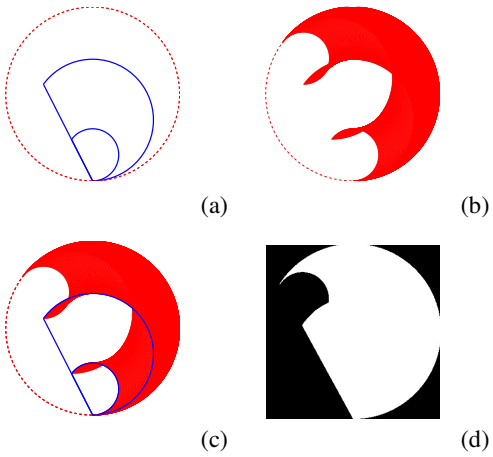

Fig. 6. Combination of R-line coverage from arc-to-arc and arc-to-line. (a) the outline of the R-line coverage from arc-to-line in the plane $z = 0.2H$. The small partial circular arc is due to the top endpoint of the line and the big one due to the bottom endpoint of the line. (b) Coverage between the two S-arcs. (c) Combination of R-line coverage of (a) and (b). (d) the numerical simulation result.

IV. Tight Line Plus Arcs

Using the R-line coverage of the elemental trajectories, we obtain the R-line coverage for the trajectory composed of two parallel S-arcs and a tight line, as illustrated in Figure 1. Recall from section III that the R-line coverage of the arc-to-arc and the arc-to-line compensate each other quite well. However, the R-line coverage of the arc-to-line has a minimum in the plane $z = 0$ while the R-arc obtained by connecting one point on the upper S-arc to the lower S-arc reaches a maximum length; the R-line coverage of the arc-line-arc is worst in the plane $z = 0$. Figure 7 illustrates the R-line coverage of the arc-line-arc in the plane $z = 0$ with source-angular coverage of 230° and 310°. As we can see, the R-lines are not fully covering the Region-of-Interest (ROI) for both angular coverages. In fact, as long as the angular coverage is less than 360°, there is always an angular space touching the z axis that is not covered by R-lines.

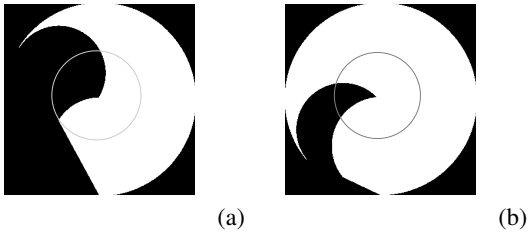

Fig. 7. Numerical simulation results of R-line coverage for two parallel circular arcs plus a tight line (ALA). (a) R-line coverage of ALA in the plane $z = 0$ with angular coverage of 230°. (b) R-line coverage of ALA in the plane $z = 0$ with angular coverage of 310°.

V. Extended Line Plus Arcs

To overcome the problem mentioned in the previous section, we here propose the trajectory composed of two parallel S-arcs and an extended line as shown in Figure 1b. In this case, the R-line coverage from an arc-to-line trajectory occupies a larger area that can offer more R-lines in the central region. How large the R-line coverage from an arc-to-line trajectory is depends on how long the line extends beyond the two S-arcs. Details will be given later in this section.

First, we would like to show the numerical simulation result of the R-line coverage for an arc-extended-line-arc trajectory with angular coverage of 230° and 310° in Figure 8. Here for the angular coverage of 230° we use $\Delta h = 0.832(2H)$ and for the angular coverage of 310° we use $\Delta h = 0.485(2H)$. The circle in the middle is the ROI corresponding to the angular coverage of 230°. Compared to the simulation results depicted in Figure 7, we can see the ROI is already fully covered.

(a) (b)

Fig. 8. Numerical simulation result of two parallel circular arcs plus an extended line (AELA). (a) R-line coverage of AELA in the plane $z = 0$ with angular coverage of 230° and $\Delta h = 0.832(2H)$. (b) R-line coverage of AELA in the plane $z = 0$ with angular coverage of 310° and $\Delta h = 0.485(2H)$.

We still have one open question: how far should we extend the line, i.e., how large Δh should be? From the analysis in seciton III, we can see that the R-line coverage of the trajectory of two parallel circular arcs plus a tight line has its minimum in the plane $z = 0$. Therefore, we only investigate here the R-line coverage for the arc- (extended)line-arc trajectory in the plane $z = 0$.

Suppose the desired ROI radius is given and denoted as $RROI$. To be practical, we calculate the fan angle using $RROI$ and denote it as α. We first start from the short scan and calculate the minimum Δh that is needed to cover the ROI; then we increase the angular coverage of the trajectory and see whether the value of Δh depends on the angular coverage or not. Figure 9a illustrates the R-line coverage of the arc-line that needed to cover the ROI. In this case, the R-line coverage from an arc-to-line trajectory has to cover the whole ROI, and thus we can calculate the minimum line extension using the following equation:

$$\frac{\Delta h}{2H} = \frac{RROI}{R - RROI} \tag{1}$$

If Δh is bigger than the value obtained from equation 1, we get additional gain of R-line coverage in the central region, as illustrated in Figure 9b.

With the increase of the angular coverage, the R-line coverage from the arc-to-arc becomes larger in the plane $z = 0$. Therefore, at some critical angular coverage, the requirement of Δh is reduced. Comparing Figure 9a and 9c, point K is the intersection between the ROI and the circle centered on the point O^i. In Figure 9a, point K is on the boundaries of the ROI and the missing R-line coverage region, but it is not the furthest such point from A^e. However, when the angular coverage increases, for example, in Figure 9b, point K is the furthest point from A^e such that it is still on the boundaries of the ROI and the missing R-line coverage region. Connecting point K and O and extending it along the direction from K to O, we get an intersection A^c, as shown in Figure 9c; we denote the corresponding angular coverage as θ_c. The requirement for Δh changes when the angular coverage pass through θ_c. Suppose now the angular coverage is greater than θ_c, as illustrated in Figure 9c, and draw a dashed circle through points K and A^e such that it is tangent to the big circle where A^i and A^e are located. Draw a line from point A^e to O and intersect this line with the dashed circle at point W. Letting the distance between O and W be R_x, we can obtain the minimum requirement of Δh using the equation below:

$$\frac{\Delta h}{2H} = \frac{r_x}{R - r_x}. \tag{2}$$

Similar to the situation in Figure 9b, if we adopt Δh larger than the requirement shown in equation 2, we get an additional gain of R-line coverage in the central region in the plane $z = 0$, as depicted in Figure 9d.

Let θ be the angular coverage, combining equations 2 and 1, we get a complete formula expressing the minimum requirement for Δh:

$$\frac{\Delta h}{2H} = \begin{cases} \frac{RROI}{R-RROI} & \pi + 2\alpha \le \theta \le \theta_c \\ \frac{r_x}{R-r_x} & \theta_c < \theta \le 2\pi \end{cases} \tag{3}$$

Figure 10 depicts the minimum requirement for Δh for different source-angular coverage according to equation 3. In the figure, three different $RROI$ are used, i.e., 0.454R, 0.300R and 0.156R. Figure 10 shows that when the angular coverage

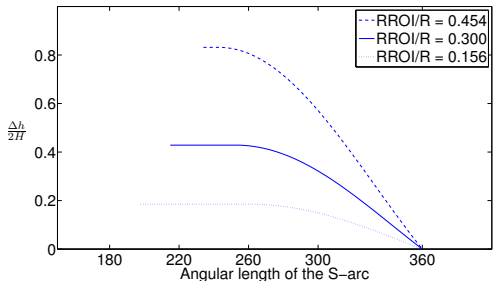

Fig. 10. Minimum Δh requirement for different angular coverage. Three $RROI$ are used, i.e., $0.454R$, $0.300R$ and $0.156R$, where R is the radius of the S-arc.

approaches 360°, the minimum requirement of Δh reduces to zero. This is consistent with the conclusion in section III that the two parallel circles plus an orthogonally attached tight line has full R-line coverage. Although there is always a Δh available to make sure that the ROI is fully covered by R-lines, it is too expensive to do so when the angular coverage is too small and the required ROI is too large, which could lead to an impractical trajectory. However, for a trajectory with large angular coverage and an ROI requirement that is not too great, the two parallel circular arcs plus an extended line does offer nice R-line coverage in the central region, while keeping the cost of line extension low.

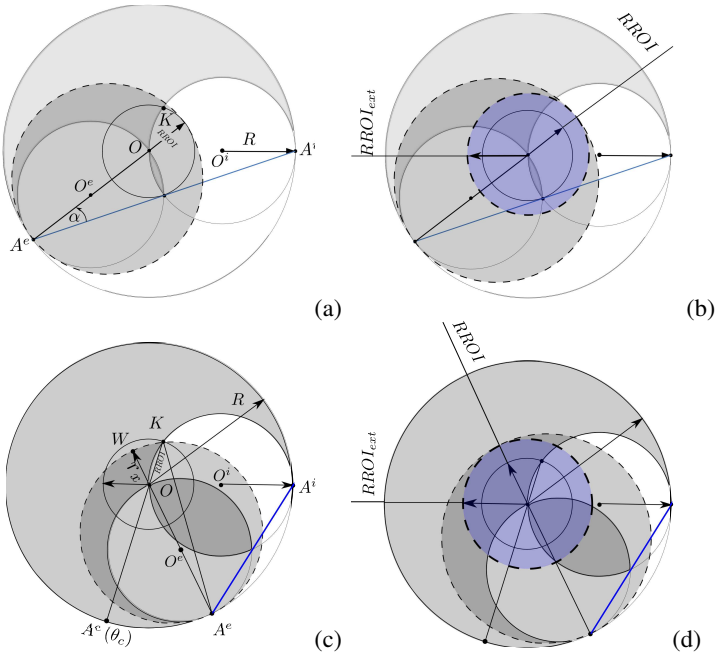

Fig. 9. Relation between Δh and $RROI$ (the desired radius of ROI), such that the R-line coverage of the arc-line covers the whole ROI in the plane $z = 0$. The minimum short scan here is design according to RROI. (a) The R-line coverage from the arc-line should at least cover the whole ROI for the minimum short scan, and we denote the corresponding extension of line as Δh_{RROI}. (b) the increase of Δh leads to the increase of central R-line coverage as described by the central dashed circle. (c) The R-line coverage from the arc-line is not necessary to cover the whole ROI thanks to the additional R-line coverage from the arc-to-arc, when the angular coverage is bigger than θ_c that corresponds to A_c in the figure. (d) As in Figure (b), the increase of Δh will give us some gain of the R-line coverage in the central region.

VI. Conclusion

We have investigated R-line coverage for a trajectory consisting of two circles connected by a line. We have observed that the R-line coverage is insufficient for a central region of interest when the line is tightly fit between the circles. On the other hand, if the line extends beyond the circle, we find the nice result that there exists a central ROI that is fully covered by R-lines. How big this central region is depends on how big Δh is. Also, we have shown that some further gain is achieved when the length of the short-scan is increased beyond its minimal value. From a practical implementation viewpoint, the line extension is not very satisfactory because it requires a short pause in exposure. One way to circumvent this problem is to replace the two S-arcs by helical arcs that touch the extended line at its endpoints as shown in Figure 11. We have done preliminary numerical simulations with this trajectory and have observed that it retains essentially the same properties of the trajectory studied in this work, while being more practical.

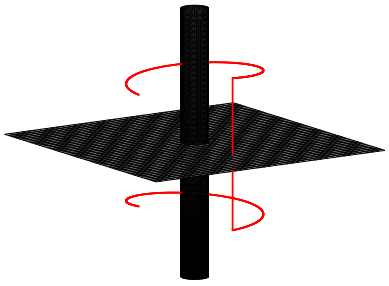

Fig. 11. Trajectory composed of two helices and a line.

References

[1] S. Cho, D. Xia, C. A. Pelizzari, and X. Pan, "Exact reconstruction of volumetric images in reverse helical cone-beam ct," *Med.Phys*, vol. 35, no. 7, pp. 3030–040, July 2008.

[2] F. Noo, A. Wunderlich, G. Lauritsch, and H. Kudo, "On the problem of axial data truncation in the reverse helix geometry," in *10th International Meeting on Fully Three-Dimensional Image Reconstruction in Radiology and Nuclear Medicine*, September 2009, pp. 90–93.

[3] A. I. Katsevich, "An improved exact filtered backprojection algorithm for spiral computed tomography," *Adv. Appl. Math*, vol. 32, no. 4, pp. 681–697, May 2004.

[4] J. D. Pack, F. Noo, and R. Clackdoyle, "Cone-beam reconstruction using the backprojection of locally filtered projections," *IEEE Trans. Med. Imaging*, vol. 24, no. 1, pp. 70–85, Jan 2005.

[5] Y. Zou and X. Pan, "Exact image reconstruction on pi-lines from minimum data in helical cone-beam ct," *Phys. Med. Biol.*, vol. 49, no. 6, pp. 941–959, Feb 2004.

[6] Y. Ye, S. Zhao, H. Yu, and G. Wang, "A general exact reconstruction for cone-beam ct via backprojection-filtration," *IEEE Trans. Med. Imaging*, vol. 24, no. 9, pp. 1190–1198, Sep 2005.